Liquid Metal-Based Tunable Linear Phase Shifters With Low Insertion Loss, High Phase Resolution, and Low Dispersion

Wu, Yi-wen; Tang, Shi-yang; Churm, James; Wang, Yi

DOI:
10.1109/TMTT.2023.3248954

Liquid Metal-Based Tunable Linear Phase Shifters With Low Insertion Loss, High Phase Resolution and Low Dispersion

Yi-Wen Wu, Shi-Yang Tang, James Churm, Yi Wang, *Senior Member, IEEE*

***Abstract*—A linear, tunable, and self-compensating phase shifter based on liquid metal (LM) is proposed in this paper using a half-mode substrate-integrated-waveguide (HMSIW). The key phase shifting element is a via-pad-slot (VPS) structure where a thru via is attached to a pad surrounded by an annular slot. This is equivalent to a shunt capacitance and inductance loaded on the HMSIW. Phase shift is achieved when the annular slot is covered by the LM that runs in microfluidic channels on the surface of the HMSIW. This allows easy implementation and convenient manipulation of the LM without incurring excessive losses. A self-compensation structure, based on multiple rows of VPSs, is proposed to achieve a low phase deviation with frequency (low dispersion). The design method to ensure a linear and small phase step over a large phase range is presented. Two phase shifters have been designed and experimentally verified. The phase shifter-I, with two VPS rows, provides a phase shift from 0 to 41° with ±1° phase deviation with frequency over 9.5 - 12.5 GHz. The average phase resolution is 1°. The measured insertion loss (IL) is 0.8 ± 0.1 dB, with a figure-of-merit of 45.6°/dB. The phase shifter-II uses three VPS rows to provide a phase shift from 0° to 180° with a phase resolution of 1.68°. The achieved phase deviation with frequency is within ±2° over 10 - 12.5 GHz and within ±5° over 9 - 13 GHz. The measured IL is 1.1 ± 0.1 dB with a competitively high figure-of-merit of 163.6°/dB. Unlike many other phase shifters, the loss of the proposed phase shifters does not increase with the phase shift. The measurements are in very good agreement with the circuit analysis and simulations. The proposed linear phase shifter has demonstrated high performance and very attractive features such as low IL that does not strongly depend on the phase shift, linear phase change, high phase resolution, and low phase dispersion with frequency. Compared with other LM-enabled phase shifters, it has the advantage of easy implementation and control. This LM-based phase shifter also potentially has high power handling capability.**

***Index Terms*— High phase resolution, linear phase modulation, liquid metal, low dispersion, low insertion loss, phase compensation, phase shifters.**

I. Introduction

PHASE shifters are a key circuit component with broad applications in signal modulation and demodulation, wireless communication, imaging, phased array antennas, and test instruments [1]. A wide range of microstrip-based phase shifters have been reported, such as Schiffman phase shifters [2]-[5], reflective-type phase shifters using 90° hybrid couplers [6]-[8], broadside-coupled phase shifters [9]-[11], stub-loaded phase shifters [12]-[16], phase shifters based on the right- and left-handed transmission lines [17]-[18], and liquid crystal-based phase shifters [19]-[20]. However, these microstrip-based phase shifters often suffer from high insertion loss (IL), low power handling capability, and spurious radiation and crosstalk especially at higher frequency bands.

Substrate-integrated waveguide (SIW) is a transmission media with lower losses and higher power handling than microstrips. SIW-based phase shifters also flourished, such as those air-hole-loaded [21]-[22], via-loaded [23]-[29], or slot-loaded [30]-[31] phase shifters. For example, the fixed phase shift can be realized by inserting air holes in the SIW, which changes the effective dielectric constant [21]-[22]. In [21], eight rows of air holes resulted in a fixed phase shift of 24.8° ± 4.7° with 0.8 dB IL over 8 - 11 GHz (32%). Preeti Yadav et al [22] extended the work in [21] by cascading a 3 dB hybrid coupler. Changing the position of the via arrays in a SIW and therefore its effective width alters the propagation constant [32]. This has been used to cause a fixed phase shift of ~180° ±6° over 10.6-11.3 GHz (6.39%) with the IL less than 1.63 dB [23]. In [24], the phase deviation of the 180° directional coupler is ±6° from 22.3 to 24.6 GHz (9.81%). As a dispersive guided-wave structure, SIW phase shifters suffer from large phase deviations over the operating frequency band. To overcome this problem, a fixed self-compensating phase shifter was proposed in [25] by taking advantage of the opposite tendencies with frequency for a delay line and an equal-length unequal-width phase shifter. A relatively small deviation of 2.5° over 45% bandwidth has been achieved for a 90° phase shifter [25]. Unlike the methods of changing the width of SIW [23]-[25], inserting vias into the SIW can also alter the phase [26]-[27]. But the bandwidth is very limited, e.g. 67.5° phase shift over only 0.32% bandwidth at 10 GHz [27]. The via inserted in the SIW can also be isolated from the ground by etching a slot around it [28]. Using this method, phase shifts with ±5° phase deviation and four fixed phase shifts were shown from 23 to 25.5 GHz (10%), and the IL is less than 1.5 dB. To reduce the phase deviation, complementary phase responses resulting from shunt and series capacitances inserted in the half-mode SIW (HMSIW) can be used [29]. Interdigital capacitor etched on the top surface of HMSIW causes a positive phase shift that decreases with frequency, whereas square patches and blind-holes introduce shunt capacitance and therefore a negative phase shift that decreases with frequency. The combined effect allows phase compensation [29], with an achieved phase shift of 43.5° ± 2.5° within 6.8-9.8 GHz (35.7%) and 86.5° ± 2.5° within 5.5-9.5 GHz (53.3%). Phase compensation means the compensation for the phase change with frequency. However, the use of blind holes requires a four-layer PCB which increases the fabrication complexity. Slotted SIW and microstrip delay lines have opposite phase slopes, which can be applied for phase compensation [30]-[31]. The phase error of a fixed 45° phase shifter is ±2.5° from 10.2 to 18.85 GHz (59.6%), while the fixed 90° phase shifter has ±5° deviation from 9.5 to 18.1 GHz (62.3%) [30]. Five 26 GHz phase shifters were reported with −90° ± 5° (26.6%), −45° ± 2.5° (29.2%), %), 45° ± 2.5° (35.8%), and 90° ± 5° (39.3%) [31]. These

Manuscript received Month DD, YYYY; revised Month DD, YYYY; accepted Month DD, YYYY.

This work was supported by UK Engineering and Physical Sciences Research Council grants EP/V008382/1. (*Corresponding author: Yi-Wen Wu*)

Y. Wu, S. Tang, J. Churm, and Y. Wang are with School of Engineering, University of Birmingham, B15 2TT, United Kingdom (e-mail: {y.wu.7, s.tang, j.r.churm, y.wang.1}@bham.ac.uk).

are all fixed phase shifters [21]-[31] with limited functionality and not suitable for reconfigurable applications.

Most tunable SIW phase shifters are realized by loading NIP, PIN, or varactor diodes [33]-[35]. Derived from the via-loaded fixed phase shifter [26]-[29], tunable phase shifters can be realized by replacing the inductive vias with NIP diodes [33] or varactor diodes [34]. By turning the NIP diodes ON and OFF, the loading state and therefore the phase of the SIW can be changed [33]. Using four NIP diodes, a maximum phase shift of 44.65° was achieved within 9.8-10.5 GHz (6.9%). The IL is less than 1.27 dB, and the average phase shift step is about 5.6° [33]. Shunt varactors can provide continuous phase shifts. Using four shunt varactors, a maximum phase shift of 31.2° is achieved within 1.6-2.6 GHz (47.6%) [34]. Its IL is less than 2.3 dB and the phase deviation is about 3° at 2.1 and 2.3 GHz. Different from the slot-loaded phase shifters in [30]-[31], transverse slots etched on the SIW were used as a reflective load in reflection-type phase shifters [35]-[36]. When a varactor diode is installed across the slot, a variable reflective load is controlled by the applied DC voltage. The phase variation is about 360° from 11.325 to 11.825 GHz (4.32%), and the IL is around 6 dB [35]. Tunable SIW phase shifters based on a high dielectric-constant slab, Barium lanthanide tetratitanates (BLT), were studied in [36]-[37]. A longitudinal slot is etched on the top surface of the SIW, and a BLT (ε_r = 100, $tan\delta$ = 0.01 at 30 GHz) slab is mounted over the slot. When the distance between the slot and the BLT slab is changed by the magnetic actuator, the electric field intensity around the slot varies and the phase changes [36]-[37]. The reported phase shift range is 275° within 29-31 GHz (6.67%), the IL is under 2.25 dB, and the phase deviation is about ± 12.5°. The use of diodes and BLT slabs requires biasing and usually increases power consumption. However, they suffer from high IL, non-linear phase shift and relatively large phase deviation.

Gallium (Ga)-based liquid metal (LM) alloys have also been used to design tunable phase shifters [38]-[40]. These LM materials are stable, non-toxic, and have excellent electrical and thermal conductivities, and low melting points. A phase shift of about 67° was realized by filling or emptying the slots of the EBG structure with LM [38]. Its IL is less than 1.8 dB at 5.6 GHz, and the phase deviation is very large. A stretchable coaxial phase shifter was demonstrated with a LM center conductor and a LM shield [39]. When it is stretched by 65 mm, the phase changes by 203° at 1.5 GHz and 461° at 3.5 GHz. This is a large phase deviation of 258° [39]. The IL is as large as 2.8 dB. Shaker Alkaraki et al [40] reported the first tunable SIW phase shifter based on LM with a maximum phase shift of 180° and a large step of 10° at 10 GHz. This was done by switching between 3 different paths that have a phase shift of 60° per path. The switch was realized by filling or emptying drilled holes in SIW with LM. The smaller step of 10° was introduced by filling or emptying six additional holes which act as reactive loading to each path [40]. The phase shifter has a high IL of 2.3 dB and high dispersion with frequency. The bandwidths for a phase deviation within ±5° and ±20° are only 160 MHz (1.6%) and 520 MHz (5.2%). The manipulation of LM through a number of vertical holes makes the phase shifter cumbersome and complicated to operate.

To overcome these challenges with LM-based phase shifters while competing with other phase shifter technologies, a novel LM-based linear, tunable and self-compensating phase shifter with all-round performance of low IL, high phase resolution and small phase deviation (low dispersion) is proposed in this paper. The central tuning element is a Via-Pad-Slot (VPS) structure where a thru via is attached to a circular pad surrounded by an annular slot. Phase shift is achieved by running LM over a series of slots in a microfluidic channel on the surface of the HMSIW. No LM goes through any vertical vias. The impact of this simple tuning mechanism on the insertion loss is minimal. It has been shown that the insertion loss does not depend on the phase shift and a high figure-of-merit of 163.6°/dB is obtained. A self-compensation structure is implemented to achieve a linear phase shift with a small phase step and a low deviation with frequency (low dispersion) over a wide band. The comparison with other state-of-the-art phase shifters [24], [29]-[40] has shown superior performance of the proposed phase shifters in terms of low insertion loss, high figure-of-merit, and low phase variation with frequency through phase compensation. Compared with other LM-based phase shifters [39]-[40], the novel VPS-based planar tuning element presents a simpler and more practical tuning solution for using LM in microwave circuits. Two prototypes with a phase range of 45° and 180° have been designed to verify the proposed method. Section II describes the operating mechanism of the phase shifter and the self-compensation technique using equivalent circuits. Section III presents two prototype designs followed by details of the fabrication and results in Section IV. Conclusions are drawn in Section V.

II. Principle of Operation

A. Via-Pad-Slot (VPS) Structure and its Equivalent Circuit

From the circuit point of view, a via (a conducting thru hole) inserted in a SIW structure is equivalent to a T-network loaded in the circuit [26]-[27]. As shown in Fig. 1, it consists of a shunt inductance, L, and a pair of series capacitances, C. The shunt inductance is produced by the via connecting the top and bottom metal layers of the SIW, while the series capacitances are produced by the coupling between the vias and the sidewalls of the SIW. The phase, θ, of the equivalent T-network can be calculated by

$$\theta = tan^{-1}\left[\frac{B+2X-BX^2}{2(1-BX)}\right], \quad (1)$$

where the susceptance $B = 1/\omega L$, and the reactance $X = 1/\omega C$. When the diameter (d) of the via is much smaller than the width (W) of the SIW, the series capacitances (C) can be negligible [28].

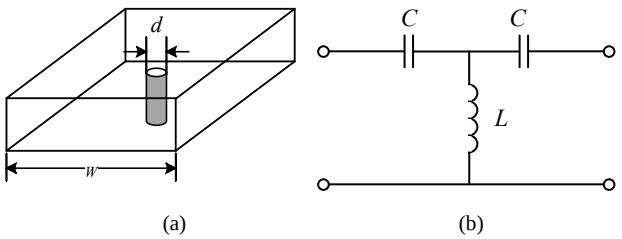

Fig. 1. (a) Structure and (b) equivalent circuit of the conventional via inserted in a SIW.

It has been shown in [29] that a blind hole with a square patch in HMSIW produces a shunt capacitance and inductance. To realize the same equivalent circuit effect, we propose a Via-Pad-Slot (VPS) structure where a thru via is attached to a circular pad surrounded by an annular slot, in the HMSIW structure as shown in Fig. 2(a). Its effective circuit is shown in Fig. 2(b). The inductances L_{s0}, L_{s1} and capacitance C_{s1} are those from the HMSIW itself, whereas the shunt inductance L_1 and shunt capacitance C_1 are produced by the VPS structure. Shown in Fig. 2(a) are two of these – VPS-I and II, together represented by L_1 and C_1. Compared with the blind-hole-patch in [29], the VPS structure is much easier to implement and only requires a single layer of the substrate. More importantly, it will become clearer later the VPS structure also simplifies the channeling of the liquid metal where the liquid only runs on the surface of the substrate without requiring any filling of vertical holes as in [41].

When the slot of VPS-I is covered by liquid metal as illustrated in Fig. 3(a), it is reduced to a normal via. Hence, the shunt capacitance associated with the slot disappears. The equivalent circuit of the resultant HMSIW with one VPS filled by the LM becomes Fig. 3(b). The shunt inductance L_2 and shunt capacitance C_2 are still produced by VPS-II, whereas the shunt inductance L_3 is from the normal via after the annular slot in VPS-I is covered by LM. It will be shown next that when the LM covers the slot, a phase shift will occur. This is the central idea of the phase shifter proposed in this work.

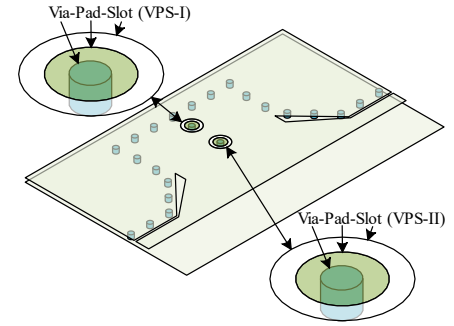

(a)

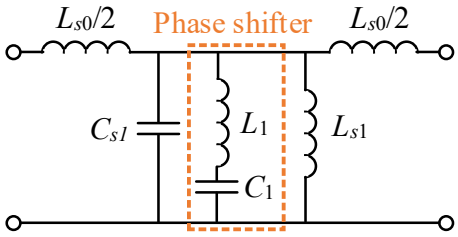

(b)

Fig. 2. The reference HMSIW with two via-pad-slot (VPS) structures. (a) Structure. (b) Equivalent circuit.

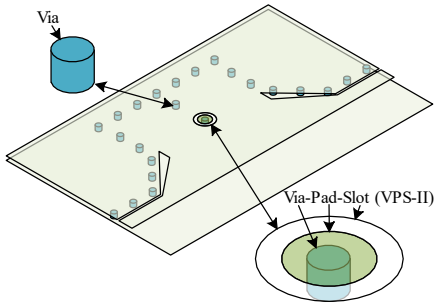

(a)

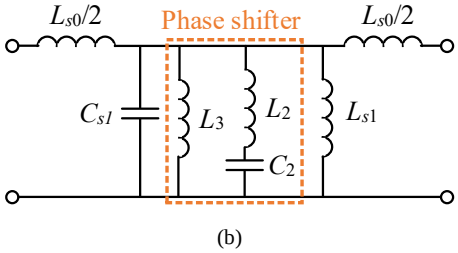

(b)

Fig. 3. The LM-loaded HMSIW with one VPS structure and one normal via. (a) Structure. (b) Equivalent circuit.

B. Theory of Self-Compensation for Low Phase Deviation With Frequency (or Low Dispersion)

When one of the via-pad-slot structures is covered by liquid metal, the phase difference between the circuits in the dotted box of Fig. 2(b) and Fig. 3(b) gives us the phase shift. Their phases can be calculated using transmission ABCD matrixes. For the circuit in Fig. 2(b), the matrix can be calculated as follows

$$Z_1 = j\omega L_1 + \frac{1}{j\omega C_1} = \frac{1-\omega^2 L_1 C_1}{j\omega C_1}, \tag{2}$$

$$Y_1 = \frac{1}{Z_1} = \frac{j\omega C_1}{1-\omega^2 L_1 C_1}, \tag{3}$$

$$\begin{bmatrix} A_1 & B_1 \\ C_1 & D_1 \end{bmatrix} = \begin{bmatrix} 1 & 0 \\ Y_1 & 1 \end{bmatrix} = \begin{bmatrix} 1 & 0 \\ \frac{j\omega C_1}{1-\omega^2 L_1 C_1} & 1 \end{bmatrix}. \tag{4}$$

The corresponding transmission coefficient, $S_{21}^{(1)}$, is

$$S_{21}^{(1)} = \frac{2}{A_1 + B_1 Y_0 + C_1/Y_0 + D_1} = [2Y_0(1-\omega^2 L_1 C_1) - j\omega C_1] \cdot \Delta_1, \tag{5}$$

$$\Delta_1 = \frac{2Y_0(1-\omega^2 L_1 C_1)}{[2Y_0(1-\omega^2 L_1 C_1)]^2 + (\omega C_1)^2}, \tag{6}$$

where Y_0 is the admittance of the HMSIW. Hence, the phase (θ_1) is

$$\theta_1(\omega) = tan^{-1}\left(\frac{-\omega C_1}{2Y_0(1-\omega^2 L_1 C_1)}\right) < 0. \tag{7}$$

Similarly, the ABCD matrix of the circuit in Fig. 3(b) can be calculated as

$$\begin{bmatrix} A_2 & B_2 \\ C_2 & D_2 \end{bmatrix} = \begin{bmatrix} 1 & 0 \\ \frac{1}{j\omega L_3} & 1 \end{bmatrix} \begin{bmatrix} \frac{j\omega C_2}{1-\omega^2 L_2 C_2} & 0 \\ 1 & 1 \end{bmatrix} = \begin{bmatrix} \frac{1}{j\omega L_3} + \frac{j\omega C_2}{1-\omega^2 L_2 C_2} & 0 \\ 1 & 1 \end{bmatrix}. \tag{8}$$

The corresponding transmission coefficient, $S_{21}^{(2)}$, is

$$S_{21}^{(2)} = [2Y_0 \omega L_3 (1-\omega^2 L_2 C_2) + j[1-\omega^2 C_2 (L_2 + L_3)]] \cdot \Delta_2, \tag{9}$$

$$\Delta_2 = \frac{2Y_0}{[2Y_0 \omega L_3 (1-\omega^2 L_2 C_2)]^2 + [1-\omega^2 C_2 (L_2+L_3)]^2}. \tag{10}$$

Hence, its phase (θ_2) is

$$\theta_2(\omega) = tan^{-1}\left(\frac{1-\omega^2 C_2 (L_2+L_3)}{2Y_0 \omega L_3 (1-\omega^2 L_2 C_2)}\right) > 0. \tag{11}$$

Since both the via and the VPS can be treated as lumped element, we have $\omega^2 L_1 C_1 \ll 1$, $\omega^2 L_2 C_2 \ll 1$, and $\omega^2 C_2 (L_2 + L_3) \ll 1$ in the operating frequency band ($\omega \in [\omega_1, \omega_2]$, where ω_1 and ω_2 are the lowest and highest operating frequencies). It can be found that $\theta_1(\omega) < 0$ while $\theta_2(\omega) > 0$. Therefore, the phase shift between the reference HMSIW (Fig. 2) and the LM-loaded HMSIW (Fig. 3) is

$$\Delta\theta(\omega) = \theta_2(\omega) - \theta_1(\omega) = tan^{-1}\left(\frac{1-\omega^2 C_2 (L_2+L_3)}{2Y_0 \omega L_3 (1-\omega^2 L_2 C_2)}\right) - tan^{-1}\left(\frac{-\omega C_1}{2Y_0 (1-\omega^2 L_1 C_1)}\right), \tag{12}$$

$$\Delta\theta(\omega) \approx tan^{-1}\left(\frac{1-\omega^2 C_2 (L_2+L_3)}{2Y_0 \omega L_3}\right) - tan^{-1}\left(\frac{-\omega C_1}{2Y_0}\right). \tag{13}$$

Normally the phase shift $\Delta\theta(\omega)$ is a function of frequency or dispersive. What concerns us here is to minimize the variation of this phase shift with frequency, i.e. to achieve low dispersion.

The phase shift variation with frequency can be expressed by its first-order derivative as follows

$$\frac{d\Delta\theta(\omega)}{d\omega} = \frac{d\theta_2(\omega)}{d\omega} - \frac{d\theta_1(\omega)}{d\omega} = \mu_2(\omega) - \mu_1(\omega), \tag{14}$$

where

$$\mu_1(\omega) = \frac{2Y_0C_1}{4{Y_0}^2+(\omega C_1)^2} > 0, \quad (15)$$

$$\mu_2(\omega) = \frac{2Y_0L_3[1+\omega^2C_2(L_2+L_3)]}{(2Y_0\omega L_3)^2+[1-\omega^2C_2(L_2+L_3)]^2} > 0. \quad (16)$$

Since the phase slope $\mu_1(\omega)$ and $\mu_2(\omega)$ of $\theta_1(\omega)$ and $\theta_2(\omega)$ have the same sign, they cancel each other, which minimizes the phase variation with frequency. This is the essence of the self-compensation mechanism. By adopting the VPS structures, a wideband phase shifter with low dispersion can be realized.

III. Design of Phase Shifters

Next, we will use two examples to demonstrate the design method, analysis and implementation of the phase shifter.

A. Phase Shifter-I (Two Rows of VPS Structures)

As shown in Fig. 4, the phase shifter-I consists of two rows of via-pad-slot structures (VPS-I and VPS-II). It should be noted that they are etched on either side of the substrate to facilitate the placement of the channels for the LM. The key dimensions are listed in Table I. It is designed on a 0.508 mm-thick Taconic TLY-5Z substrate (ε_r=2.21) [42] with 35 μm-thick copper. The individual via-pad-slot structures for VPS-I and VPS-II have the same dimensions. It is important to note that the row of VPS-I is used for tuning the phase whereas the VPS-II row is there for the phase compensation, as discussed in Section II-B, to realize a wideband phase shifter with low dispersion. When the slots of VPS-I are covered by LM one by one, the phase can be step-tuned. To demonstrate the design step, the VPS dimensions are investigated by full-wave parameter simulation, as depicted in Fig.

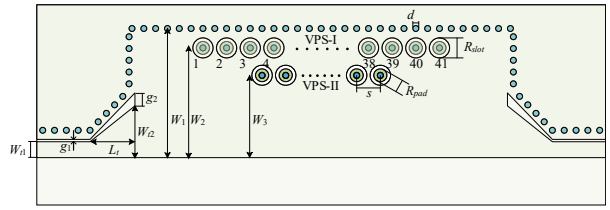

(a)

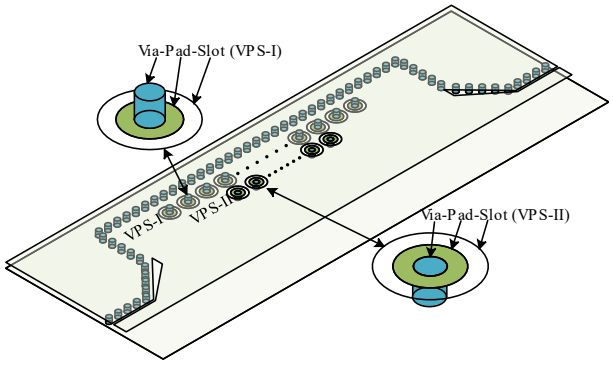

(b)

Fig. 4. Topology of the tunable phase shifter-I (not to scale). (a) Top view. (b) 3D view.

TABLE I
Geometries of the Proposed Phase Shifter-I (Unit: mm)

W_1	W_2	W_3	W_{t1}	W_{t2}	L_t
11	9.35	8	1.35	4.4	3.8
g_1	g_2	R_{slot}	R_{pad}	s	d
0.2	1.1	0.93	0.53	1	0.25

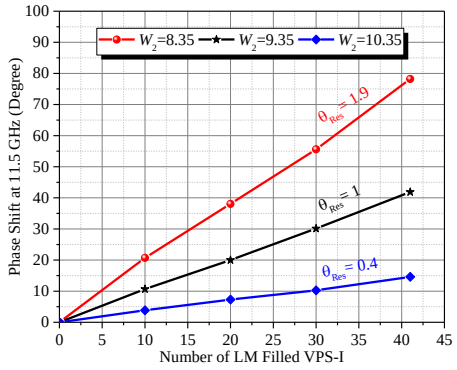

(a)

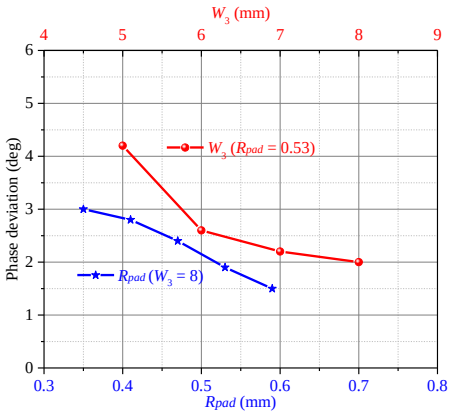

(b)

Fig. 5. Parameter studies. (a) W_2. (b) W_3 and R_{pad}. (The other parameters are listed in table I.)

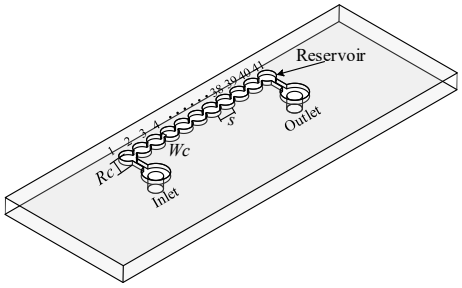

Fig. 6. Microfluidic channel used to contain LM in Phase Shifter-I.

5. The position (W_2) of VPS-I is the key to determine the maximum phase shift (θ_{Max}) and phase resolution (θ_{Res}). Fig. 5(a) presents the phase shift at 11.5 GHz for different W_2. A smaller W_2 results in a larger θ_{Max} and lower θ_{Res}. So, the first step in the design is to select an appropriate W_2 according to the desired phase resolution. Then, the numbers of required VPS structures will be determined by the maximum phase shift and phase resolution. The maximum achievable phase shift depends on the width (W_1) of the HMSIW, the location (W_2) of the VPS-I row and the number of VPSs in the VPS-I row (N_1 = 41 in this case). Generally, with a chosen W_1, a smaller W_2 and a larger N_1 lead to a larger maximum phase shift. Since the phase shift increases linearly with the number of VPSs filled with LM, as shown in Fig. 5(a), the number (N_1) of VPS-I can be calculated according to the desired θ_{Max} and θ_{Res}, i.e., $N_1 \approx \theta_{Max}/\theta_{Res}$. For the impedance matching purpose, the row of VPS-II is designed with fewer VPS structures to form a tapered structure, i.e., the numbers in the VPS-II row $N_2 = N_1 - 5$. Next, the location, W_3, of the VPS-II row is optimized

to achieve a good phase compensation. As shown in Fig. 5(b), the phase deviation gradually decreases as W_3 increases from 5 to 8 mm. In addition, as R_{pad} increases, the phase deviation also decreases due to the increased equivalent capacitance of VPS structure. Finally, a grounded coplanar waveguide (GCPW)-to-HMSIW transition is utilized for the excitation.

The microfluidic channel that is used to contain the LM is shown in Fig. 6. It consists of N_1 (41) small reservoirs and the inlet/outlet. Adjacent reservoirs are connected by narrowed channels (W_c = 0.3 mm). This feature uses the surface tension of the LM to hold it in place when there is no external pressure and requires additional pressure to overcome the resistance and fill the reservoir one after another. This allows more stable and accurate control of the phase tuning. The microfluidic channel is made with polydimethylsiloxane (PDMS) by soft lithography technology. Its dielectric constant is about 2.67 and PDMS has a relatively high loss tangent (e.g. 0.04 at 77 GHz) [43]. In this SIW phase shifter, the only open structure is the annular slot of a 0.2 mm gap on the ground of the SIW. The electromagnetic leakage through the slots is negligible. Hence the exposure of the PDMS to electromagnetic waves is minimal and does not affect the RF performance of the phase shifters. This is one of the major advantages of this VPS based phase shifter.

The simulated results of the phase shifter-I are presented in Fig. 7. As the number of LM filled VPS structures increases, the phase shift (grey shaded area in Fig. 7(a)) linearly increases from 0° to 42° at an average step of 1.02°/VPS. The phase deviation with frequency is

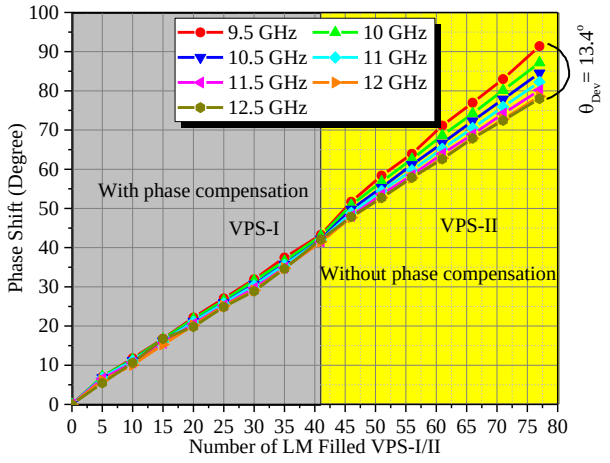

(a)

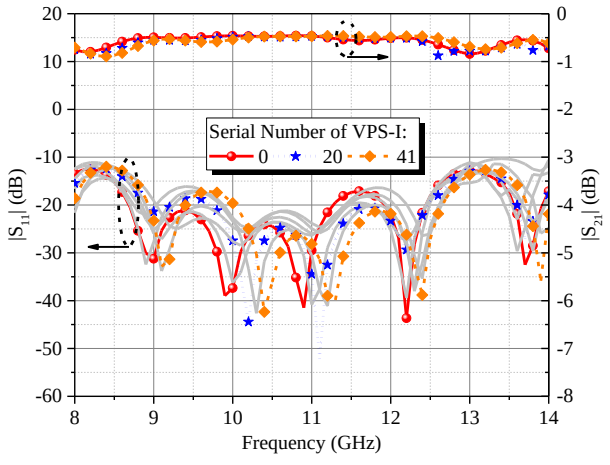

(b)

Fig. 7. Simulated results of the phase shifter-I. (a) Phase shift. (b) Reflection and transmission coefficients.

within ±1° from 9.5 to 12.5 GHz. The phase deviation is calculated by subtracting the minimum phase shift from the maximum phase shift in the operating frequency band at the maximum phase shift states. The simulated insertion loss is less than 0.55 dB at 11.5 GHz, and does not increase with the phase shift as shown in Fig. 7(b). The phase shifter has the merits of low IL, small phase shift step and phase deviation, and planar actuation of LM.

The second row (VPS-II) is primarily for phase compensation. It can be used to extend the phase shift if they are gradually covered by LM too. However, the phase deviation with frequency will increase as it loses its function for phase compensation. This is evident from the simulation results (yellow shaded area in Fig. 7(a)). Next, we will explain how we can estimate this phase deviation.

When the whole row of the VPS structures is covered by LM, it becomes a row of shorted vias. This effectively moves the sidewall of the HMSIW. So, when the VPS-I row is filled, the width of the HMSIW can be approximated by W_2 (see the definition of W_1, W_2 and W_3 from Fig. 4). When the VPS-II row is all filled by LM, this can be approximated by W_3. The change of the SIW width alters the guided wavelength as

$$\lambda_g(W_i,\omega)=\frac{\lambda}{\sqrt{1-\left(\frac{\lambda}{4W_i}\right)^2}}=\frac{2\pi c_0}{\sqrt{\omega^2-\left(\frac{\pi c_0}{2W_i}\right)^2}}, \tag{18}$$

where $W_i \in (W_1, W_2, W_3)$, $\lambda=\frac{2\pi c_0}{\omega}$ and c_0 is the speed of light in vacuum. The propagation constant becomes

$$\beta(W_i,\omega)=\frac{2\pi}{\lambda_{g(W_i,\omega)}}=\frac{\sqrt{\omega^2-\left(\frac{\pi c_0}{2W_i}\right)^2}}{c_0}. \tag{19}$$

So, the corresponding phase is $\theta(W_i,\omega)=\beta(W_i,\omega)K_i$. Note that K_i is the length of the sidewall with a width of W_i. It can be seen that extra phase deviation between ω_1 and ω_2 can be approximated by

$$\Delta\theta=\left[\left(\beta_{(W_2,\omega_2)}-\beta_{(W_3,\omega_2)}\right)-\left(\beta_{(W_2,\omega_1)}-\beta_{(W_3,\omega_1)}\right)\right]\cdot K_3, \tag{20}$$

where $\beta_{(W_i,\omega_1)}$ and $\beta_{(W_i,\omega_2)}$ are the propagation constants at frequencies ω_1 and ω_2, respectively. For example, when the slots of VPS-II are filled by LM, the position of the sidewall is moved from W_2 to W_3, and the total length of VPS-II is $K_3=(N_2-1)\times s$ = 35 mm. The extra phase deviation between 9.5 GHz and 12.5 GHz can be estimated as (when W_2 = 9.35 mm, W_3 = 8mm, f_1 = 9.5 GHz, f_2 = 12.5 GHz, K_3 = 35 mm)

$$\Delta\theta = 14.5°. \tag{21}$$

From Fig. 7(a), the simulated phase deviation (in the yellow shaded area) between 9.5 GHz and 12.5 GHz, without phase compensation is 13.4°, close to the estimation from (18)-(21).

B. Phase Shifter-II (Three Rows of VPS Structures)

As mentioned in Section III-A, a smaller W_2 and a larger N_1 will lead to a larger maximum phase shift. However, there is a trade-off. A smaller W_2 also results in an increased phase step and a larger N_1 would increase the circuit size. The row of VPS-II could be utilized to increase the phase shift. However, the phase deviation would deteriorate due to the lack of phase compensation.

To reconcile these trade-offs, a tunable phase shifter-II is proposed. It has three rows of VPS structures offering a maximum phase shift of 180°. As shown in Fig. 8, the two rows of circular VPS structures (VPS-I and VPS-II) are designed to give a 0~180° phase shift. The first row has 61 VPSs (1 to 61), and the second row has 46 VPSs (62 to 107). Again, the two rows have different lengths for impedance matching purpose. The third row of VPS-III is added for phase compensation. Different from the previous VPS structures, they have

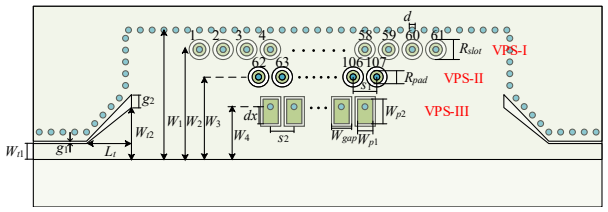

(a)

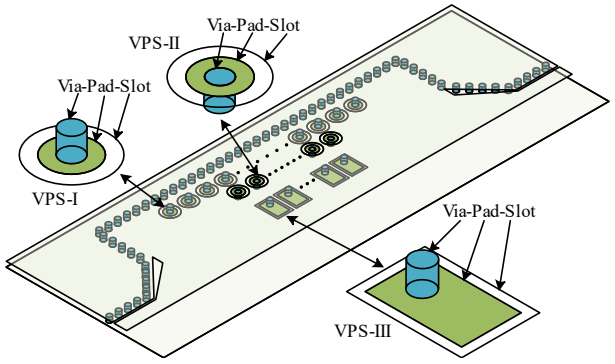

(b)

Fig. 8. Topology of the tunable phase shifter-II. (a) Top view. (b) 3D view.

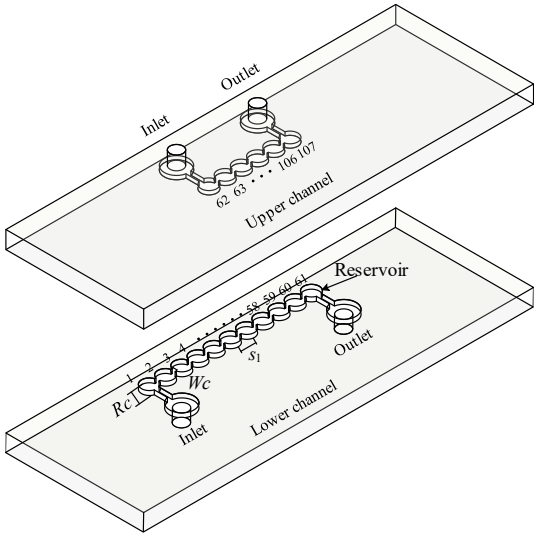

Fig. 9. Microfluidic channels used in Phase Shifter-II.

a square patch and a square slot. The purpose is to increase the shunt capacitance of the VPS by increasing the circumference of the slot (W_{gap}=1.52 mm, W_{p1}=1.1mm, W_{p2}=1.9mm). Assume $\beta(W_1,\omega_0)$, $\beta(W_2,\omega_0)$ and $\beta(W_3,\omega_0)$ are the propagation constants at the centre frequency ω_0 when the effective widths of the HMSIW are W_1, W_2 and W_3, respectively, as in (19). In order to maintain the same linear step change of the phase when filling the slots of the VPS-I and VPS-II structures, the propagation constants should satisfy the following relation

$$\beta(W_1,\omega_0)-\beta(W_2,\omega_0)=\beta(W_2,\omega_0)-\beta(W_3,\omega_0). \quad (22)$$

This is so that the propagation constant change introduced by filling the VPS-I row (the left-hand side of (22)) is the same as the propagation constant change introduced by filling the VPS-II row (the right-hand side). Using (22), when the widths W_1 and W_2 are fixed, the width W_3 can be determined from

TABLE II
GEOMETRIES OF THE PROPOSED PHASE SHIFTER-II (UNIT: MM)

W_1	W_2	W_3	W_4	W_{t1}	W_{t2}
9.7	7.935	6.5	4.5	1.35	4.2
s_1	s_2	W_{qap}	W_{p1}	W_{p2}	L_t
1	2	1.52	1.1	1.9	3.8
g_1	g_2	R_{slot}	R_{pad}	d	dx
0.2	1.1	0.93	0.53	0.25	1.35

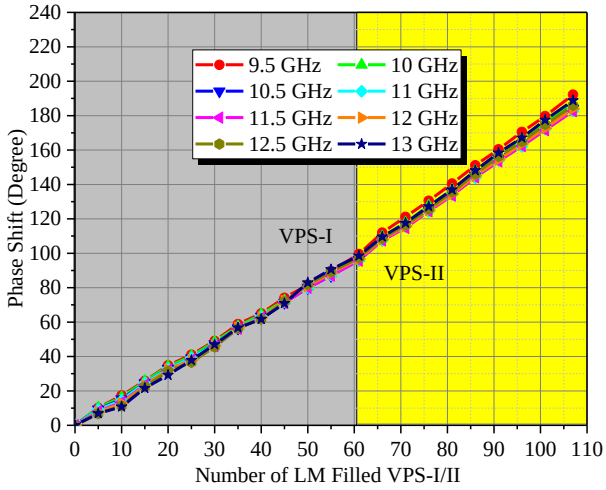

(a)

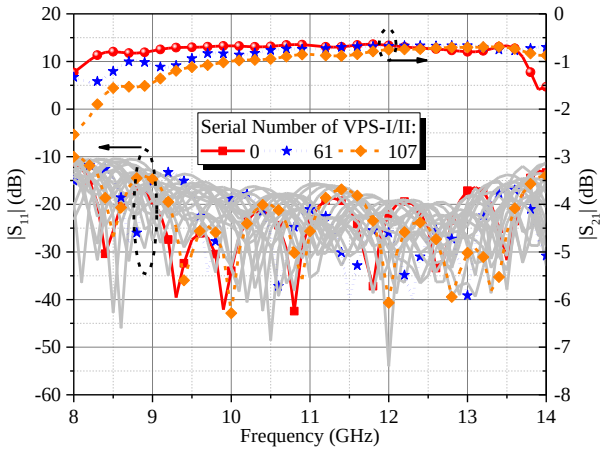

(b)

Fig. 10. Simulated results of phase shifter-II. (a) Phase shift at different frequencies. (b) Reflection and transmission coefficients.

$$\beta(W_3,\omega_0)=2\beta(W_2,\omega_0)-\beta(W_1,\omega_0). \quad (23)$$

So,

$$W_3=\frac{\pi c_0}{2\sqrt{\omega_0{}^2-\beta_{(W_3,\omega_0)}{}^2 c_0{}^2}}. \quad (24)$$

Based on (22)-(24), the widths W_1, W_2 and W_3 are chosen to keep the linear phase shift with the same step change when filling both the VPS-I and VPS-II rows. The location, W_4 (see Fig. 8(a)), and dimensions, W_{gap} and W_{p2}, of the VPS-III row are optimized to achieve a good phase compensation. As depicted in Fig. 9, two microfluidic channels are used to hold and control the LM. 61 reservoirs in the lower channel cover the VPS-I structures (1, 2, …, 61) and 46 reservoirs in the upper channel cover the VPS-II structures (62, 63, …,107). The optimized dimensions of the phase shifter-II are

given in Table II.

Fig. 10 shows the simulated results of the phase shifter-II. As the number of reservoirs in the first row filled by LM increases from 0 to 61, the phase linearly increases from 0° to 96.6° with an average step of 1.58°/VPS. The phase deviation with frequency (dispersion) is within ±1.5° from 9 to 13 GHz. When the second row is filled by the LM, the phase increases linearly from 96.6° to 184° at a step of 1.9°/VPS. The incremental rate is designed to be close to that of the first segment by carefully choosing W_3. The phase deviation with frequency is less than ±2° within 10-12 GHz. The simulated reflection coefficient is less than -10 dB from 8 to 13 GHz, and the IL is 0.8 ± 0.1 dB.

IV. Fabrication and Measurement

As shown in Fig. 11, the proposed phase shifters are fabricated by PCB technology with PDMS microfluidic channels. To avoid the leak of LM through the vias, all the vias are filled with resin. Using the plasma bonding method, the microfluidic channel of the phase shifter-I is bonded to the lower surface of the PCB circuit (Fig. 11(a)). As for the phase shifter-II, the two microfluidic channels are bonded to lower and upper surfaces of the PCB (Fig. 11(b)), respectively. Because the focus of this paper is on the novelty of phase shifters, manual actuation is utilized in the measurement for the demonstration purpose. Measurement results show stable control of the LM filling the reservoirs with the help of the bistable latching structure.

To speed up the measurement process, the VPS-I structures are filled in steps of 5 slots. When the microfluidic channels are gradually filled with LM using a syringe, the phase shift increases linearly from 0° to the maximum. The measurement results of phase shifter-I are shown in Fig. 12. The measured $|S_{11}|$ is better than -10 dB over 8-14 GHz under all LM filling states. The IL is 0.8 ± 0.1 dB at 11.5 GHz, and does not increase with the phase shift. The maximum phase shift is 41°, and the average phase shift step is 1.0°/VPS. The phase deviation with frequency is ±1° within 9.5-12.5 GHz (26%). The measured results agree well with the simulated ones.

The measurement results of phase shifter-II are shown in Fig. 13. Under various LM filling states, the measured $|S_{11}|$ is less than −10 dB over 8-14 GHz. The IL is 1.1 ± 0.1 dB at 11.5 GHz and again does not increase with the increasing phase. When VPS-I structures are filled by LM, the phase shift ranges from 0° to 96.3°, and the average phase step is 1.58°/VPS. The fractional bandwidth (FBW) is 36% (9-13 GHz) for a phase deviation of ±1.5°, and 42% (8.5-13 GHz) for a phase deviation of ±2°. When both VPS-I and VPS-II structures are utilized to tune the phase shift, the phase ranges from 0° to 180°, and the

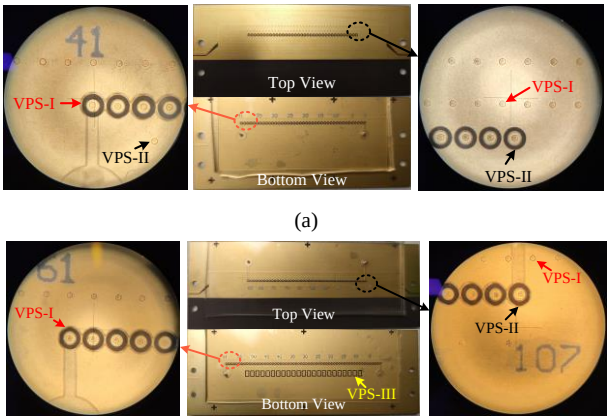

Fig. 11. Fabricated prototypes. (a) Phase shifter-I. (b) Phase shifter-II.

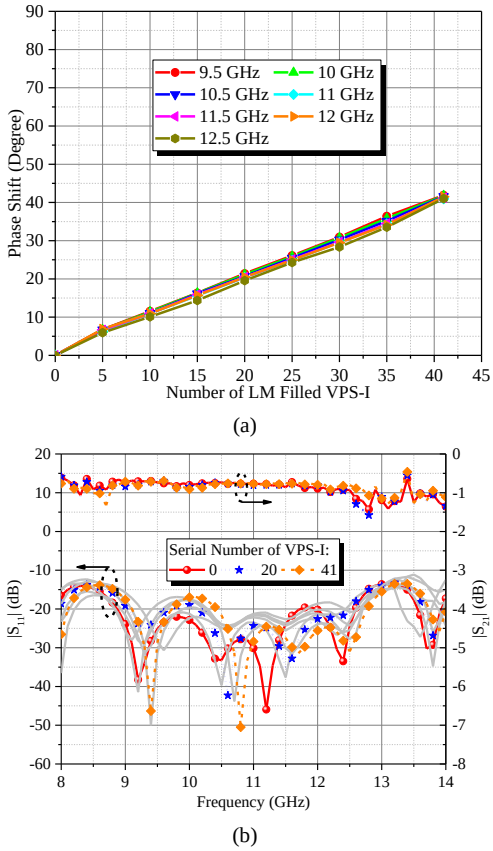

Fig. 12. Measured results of phase shifter-I. (a) Phase shift. (b) Reflection and transmission coefficients.

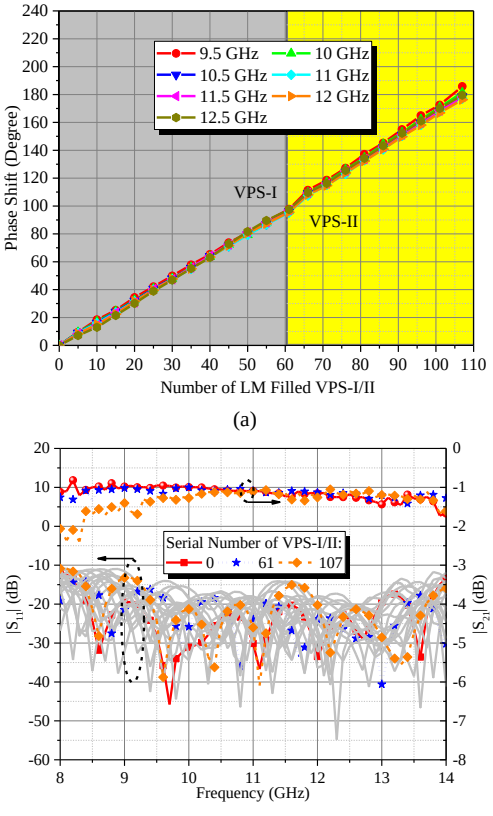

Fig. 13. Measured results of phase shifter-II. (a) Phase shift. (b) Reflection and transmission coefficients.

TABLE III
COMPARISONS OF PERFORMANCES BETWEEN THE PROPOSED AND REPORTED PHASE SHIFTERS IN LITERATURE

Reference	f_0 (GHz)	*Phase shift range* (°)	*Phase deviation* (°) [1]	*FBW* (%)	*Phase resolution* (°)	*Tunable/ Linear tuning*	*IL(dB)*	*FoM* (°/dB)[2]	*Technology*	*Typical Switching Time*[3]
[24]	10.95	180	N.A.	6.4	N.A.	No/No	~1.4	0	SIW	N.A.
[29]	24.25	60	±5	10.3	N.A.	No/No	~1.5	0	SIW	N.A.
[30]	8.3	43.5	±2.5	35.7	N.A.	No/No	~0.63	0	SIW	N.A.
	7.5	86.5	±2.5	53.3	N.A.	No/No	~1.32	0	SIW	N.A.
[32]	26	90	±5	39.3	N.A.	No/No	~0.9±0.43	0	SIW+ Microstrip	N.A.
[33]	10.15	44.7	N.A.	6.9	6.7	Yes/No	~1.27	0	SIW+NIP diodes	ns
[35]	11.58	0~180	N.A.	4.3	Continuous	Yes/No	~6	30	SIW+ Varactors	ns
[37]	30	0~275	±12.5	6.7	Continuous	Yes/No	~1.5±0.5	137.5	SIW+ BLT slab	us
[39]	2.5	0~321	±140	80	Continuous	Yes/Yes	~2.8	114.6	Coaxial line+LM	s
[40]	10	0~180	±20	5.2	10	Yes/Yes	~2.3	78.2	SIW+LM	ms~s
This work	**11.5**	**0~41**	**±1**	**26.1**	**1**	**Yes/Yes**	**~0.8±0.1**	**45.6**	**SIW+LM**	**ms~s**
		0~180	**±2**	**22.2**						
			±5	**36.4**	**1.68**	**Yes/Yes**	**~1.1±0.1**	**163.6**	**SIW+LM**	**ms~s**

Note: 1. Defined as the deviation range of the phase shifts at the operating frequency band compared to the phase shift at the center frequency in the same state.
2. Figure-of-merit (FoM) = Maximum relative phase shift / Maximum insertion loss (°/dB).
3. Typical switching time is estimated according to [44].

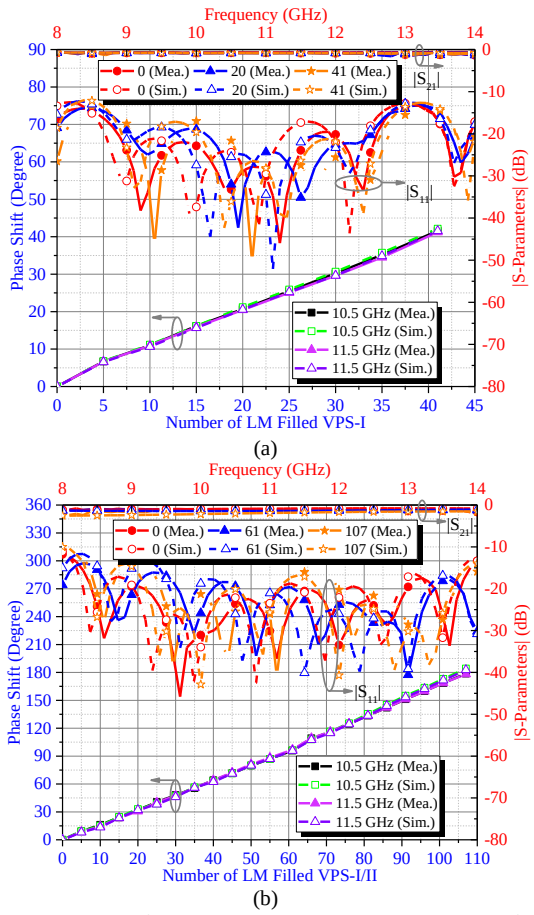

Fig. 14. Comparison of the simulated and measured phase shift and S-parameters. (a) Phase shifter-I and (b)Phase shifter-II.

average phase shift step is 1.68°/VPS. The FBW is 22% (10-12.5 GHz) for a phase deviation of ±2°, and 36% (9-13 GHz) for a phase deviation of ±5°. The measured and simulated results are in good agreement, as depicted in Fig. 14. Due to the existence of surface tension of the LM, the slots of a 0.2 mm gap in the VPS structures might not be completely filled by LM, which could have led to a higher phase deviation than expected. However, the LM can still bridge the gap and connect the pad to the metal ground to achieve a good interconnection effect.

The performance between the proposed and other reported phase shifters in the literature is compared in Table III. The proposed phase shifters have exhibited significant advantages of low insertion loss almost independent of the phase delay, high phase resolution, small phase deviation with frequency and linear phase tuning. These are resulted from a combination of features: (1) Since the LM is only used to cover the narrow slots of the VPS structures on the outside of the HMSIW and does not disturb its internal structure, its impact on the insertion loss is minimal, compared with other technologies such as diode, ferroelectric based phase shifters or those based on vertical LM vias. (2) The phase resolution of the phase shifter can be flexibly designed by controlling the dimensions and position of VPS structures. (3) The compensation mechanism using additional VPS structures leads to a low phase deviation with frequency. The phase shifter can be designed almost dispersion-less over the concerned band. (4) By varying the number of VPS structures covered by the LM, the phase shift can be linearly regulated. In addition, the phase shifter adopts a planar movement/actuation structure for the LM, which is much simpler to implement and has minimum influence on the RF performance as compared with other LM enabled phase shifters [39].

V. CONCLUSION

This paper proposes and demonstrates a X-band LM-based linear tunable HMSIW phase shifter with low insertion loss, high phase resolution, and small phase deviation. The equivalent circuit model

and the design method have been presented. The linear phase shift is realized by covering the VPS structures, the key phase shifting elements, by LM. Since the LM material does not enter the interior of the HMSIW structure, there is no excessive loss introduced in HMSIW which results in a low IL characteristic. The measurement results show that two phase shifters have an IL of 0.8 ± 0.1 dB and 1.1 ± 0.1 dB at 11.5 GHz. The insertion losses of the proposed phase shifter do not strongly depend on the phase, partly because the VPS element has low loss itself and partly because the cover of the slot by the LM eliminates the radiation loss (albeit small) from the VPS and offsets the increased conductor loss with the increasing phase. The work also shows the phase resolution of the phase shifter can be flexibly controlled and phase linearity over a large range can be ensured by design. A high resolution of 1.68° is achieved for the 180° phase shifter-II. Another key feature of the phase shifter is its passive self-compensation structure that enables low phase deviation with frequency. By further optimization, it could allow an even wider band dispersion-less phase shift.

The implementation and control of the LM have been a major challenge for a lot of LM enabled devices for the complexity introduced by the channels/tubes and the actuation mechanism. This work does not intend to address the actuation aspect, but the VPS structure used in this work only requires LM to run on the surface (the ground plane) of SIW, which presents a simple and convenient structure for fabrication as well as for the manipulation of the LM material. What is also not addressed in this work is the tuning speed of the phase shifter, which is one limitation of LM based tunable devices. The microfluidic channels used in this work aim for the conventional pneumatic or hydraulic control of LM. However, there are other electrical or magnetic actuation methods that can be explored [45]. Power handling is another interesting area for future investigation. It is plausible to expect the LM based device has high power handling capability for its resemblance to mechanical tuning without any semiconductor or thin-film materials involved. However, what cannot be completely ruled out is the potential interfacial/junction effect between LM and normal metal in the circuits. More experimental work is needed.

REFERENCES

[1] A. Singh and M. K. Mandal, "Electronically tunable reflection type phase shifters," *IEEE Trans. Circuits Syst.* II: Express Briefs, vol. 67, no. 3, pp. 425-429, March 2020, doi: 10.1109/TCSII.2019.2921036.

[2] J. L. R. Quirarte and J. P. Starski, "Novel Schiffman phase shifters," *IEEE Trans. Microw. Theory Tech*.., vol. 41, no. 1, pp. 9-14, Jan. 1993, doi: 10.1109/22.210223.

[3] W. Zhang *et al*., "A modified coupled-line Schiffman phase shifter with short reference line", *Prog. Electromagn. Res. C*, vol. 54, 17-27, 2014, doi:10.2528/PIERC14063003.

[4] L. -L. Qiu, L. Zhu, and Y. -P. Lyu, "Schiffman phase shifters with wide phase shift range under operation of first and second phase periods in a coupled line," *IEEE Trans. Microw. Theory Tech*.., vol. 68, no. 4, pp. 1423-1430, April 2020, doi: 10.1109/TMTT.2019.2953842.

[5] P. K. Deb, T. Moyra, and B. K. Bhattacharyya, "Design of compact wideband 90° Schiffman phase shifter incorporating CSRR," *Electromagnetics*, vol. 40, no. 3, pp. 207-216, Feb. 2020, doi: doi.org/10.1080/02726343.2020.1726072.

[6] C. -S. Lin, S. -F. Chang, C. -C. Chang and Y. -H. Shu, "Design of a reflection-type phase shifter with wide relative phase shift and constant insertion loss," *IEEE Trans. Microw. Theory Tech*.., vol. 55, no. 9, pp. 1862-1868, Sept. 2007, doi: 10.1109/TMTT.2007.903346.

[7] B. Biglarbegian, M. R. Nezhad-Ahmadi, M. Fakharzadeh and S. Safavi-Naeini, "Millimeter-wave reflective-type phase shifter in CMOS technology," *IEEE Microw. Wirel. Compon. Lett.*., vol. 19, no. 9, pp. 560-562, Sept. 2009, doi: 10.1109/LMWC.2009.2027065.

[8] W. Li *et al*., "A Ka-band reflection-type analog electrically controlled phase shifter," *AIP Conf. Proc.*, vol. 1820, no. 1, AIP Publishing LLC, 2017.

[9] A. M. Abbosh, "Ultra-wideband phase shifters," *IEEE Trans. Microw. Theory Tech*.., vol. 55, no. 9, pp. 1935-1941, Sept. 2007, doi: 10.1109/TMTT.2007.904051.

[10] A. M. Abbosh, "Broadband fixed phase shifters," *IEEE Microw. Wirel. Compon. Lett*.., vol. 21, no. 1, pp. 22-24, Jan. 2011, doi: 10.1109/LMWC.2010.2079320.

[11] M. Sorn, R. Lech and J. Mazur, "Simulation and experiment of a compact wideband 90° differential phase shifter shifters," *IEEE Trans. Microw. Theory Tech*.., vol. 60, no. 3, pp. 494-501, March 2012, doi: 10.1109/TMTT.2011.2175244.

[12] X. Tang and K. Mouthaan, "Phase-shifter design using phase-slope alignment with grounded shunt λ/4 stubs," *IEEE Trans. Microw. Theory Tech*.., vol. 58, no. 6, pp. 1573-1583, June 2010, doi: 10.1109/TMTT.2010.2049168.

[13] S. Y. Zheng, W. S. Chan and K. F. Man, "Broadband phase shifter using loaded transmission line," *IEEE Microw. Wirel. Compon. Lett*.., vol. 20, no. 9, pp. 498-500, Sept. 2010, doi: 10.1109/LMWC.2010.2050868.

[14] S. H. Yeung, Q. Xue and K. F. Man, "Broadband 90° differential phase shifter constructed using ap of multisection radial line stubs," *IEEE Trans. Microw. Theory Tech*.., vol. 60, no. 9, pp. 2760-2767, Sept. 2012, doi: 10.1109/TMTT.2012.2204899.

[15] L. Guo and A. Abbosh, "Phase shifters with wide range of phase and ultra-wideband performance using stub-loaded coupled structure," *IEEE Microw. Wirel. Compon. Lett*.., vol. 24, no. 3, pp. 167-169, March 2014, doi: 10.1109/LMWC.2013.2293658.

[16] J. Wang, Z. Shen, and L. Zhao, "UWB 90° phase shifter based on broadside coupler and T-shaped stub," *Electron. Lett.*, vol. 52, no. 25, pp. 2048-2050, 2016.

[17] I.-H. Lin, M. DeVincentis, C. Caloz and T. Itoh, "Arbitrary dual-band components using composite right/left-handed transmission lines," *IEEE Trans. Microw. Theory Tech*.., vol. 52, no. 4, pp. 1142-1149, April 2004, doi: 10.1109/TMTT.2004.825747.

[18] D. Kholodnyak, E. Serebryakova, I. Vendik and O. Vendik, "Broadband digital phase shifter based on switchable right- and left-handed transmission line sections," *IEEE Microw. Wirel. Compon. Lett*.., vol. 16, no. 5, pp. 258-260, May 2006, doi: 10.1109/LMWC.2006.873593.

[19] D. Wang, E. Polat, H. Tesmer, R. Jakoby and H. Maune, "Highly miniaturized continuously tunable phase shifter based on liquid crystal and defected ground structures," *IEEE Microw. Wirel. Compon. Lett*.., vol. 32, no. 6, pp. 519-522, June 2022, doi: 10.1109/LMWC.2022.3142410.

[20] D. Wang, E. Polat, H. Tesmer, H. Maune and R. Jakoby, "Switched and Steered Beam End-Fire Antenna Array Fed by Wideband Via-Less Butler Matrix and Tunable Phase Shifters Based on Liquid Crystal Technology," *IEEE Trans. Antennas Propag*., vol. 70, no. 7, pp. 5383-5392, July 2022, doi: 10.1109/TAP.2022.3142334.

[21] P. Yadav, S. Mukherjee and A. Biswas, "Design of planar substrate integrated waveguide (SIW) phase shifter using air holes," in *Proc. IEEE Appl. Electromagn. Conf.*, Guwahati, India, Dec. 2015, pp. 1–2, doi: 10.1109/AEMC.2015.7509117.

[22] P. Yadav, S. Mukherjee and A. Biswas, "Design of SIW variable phase shifter for beam steering antenna application," in *Proc. IEEE Int. Symp. Antennas Propag. (APSURSI)*, Fajardo, PR, USA, 2016, pp. 1223-1224, doi: 10.1109/APS.2016.7696319.

[23] B. Liu, W. Hong, Z.-C. Hao and K. Wu, "Substrate integrated waveguide 180-degree narrow-wall directional coupler," in *Proc. Asia–Pacific Microw. Conf. (APMC)*, Suzhou, China, Dec. 2005, 2005, doi: 10.1109/APMC.2005.1606319.

[24] Y. Cheng, W. Hong and K. Wu, "Novel Substrate Integrated Waveguide fixed phase shifter for 180-degree Directional Coupler," 2007 IEEE/MTT-S International Microwave Symposium, 2007, pp. 189-192, doi: 10.1109/MWSYM.2007.380322.

[25] Y. J. Cheng, W. Hong and K. Wu, "Broadband self-compensating phase shifter combining delay line and equal-length unequal-width phaser," *IEEE Trans. Microw. Theory Tech*.., vol. 58, no. 1, pp. 203-210, Jan. 2010, doi: 10.1109/TMTT.2009.2035942.

[26] K. Sellal, L. Talbi, T. Denidni and J. Lebel, "A new substrate integrated waveguide phase shifter," in *Proc. Eur. Microw. Conf.*, Manchester, U.K., 2006, pp. 72-75, doi: 10.1109/EUMC.2006.281184.

[27] K. Sellal, L. Talbi, and T. A. Denidni, and J. Lebel, "Design and implementation of a substrate integrated waveguide phase shifter," *IET*

Microwaves, Antennas & Propagation, vol. 2, no. 2, pp. 194-199, April 2008.

[28] T. Yang, M. Ettorre and R. Sauleau, "Novel phase shifter design based on substrate-integrated-waveguide technology," *IEEE Microw. Wirel. Compon. Lett..*, vol. 22, no. 10, pp. 518-520, Oct. 2012, doi: 10.1109/LMWC.2012.2217122.

[29] Y. Peng and L. Sun, "A compact broadband phase shifter based on HMSIW evanescent mode," *IEEE Microw. Wirel. Compon. Lett..*, vol. 31, no. 7, pp. 857-860, July 2021, doi: 10.1109/LMWC.2021.3077379.

[30] H. Peng, X. Xia, S. O. Tatu, and T. Yang, "An improved broadband siw phase shifter with embedded air strips," *Progress In Electromagnetics Research C (PIERC)*, vol. 67, pp. 185-192, 2016.

[31] W. Zhang, Z. Shen, K. Xu and J. Shi, "A compact wideband phase shifter using slotted substrate integrated waveguide," *IEEE Microw. Wirel. Compon. Lett..*, vol. 29, no. 12, pp. 767-770, Dec. 2019, doi: 10.1109/LMWC.2019.2949681.

[32] D. M. Pozar, Microwave Engineering, 3rd ed. New York: Wiley, 2005.

[33] K. Sellal, L. Talbi, and M. Nedil, "Design and implementation of a controllable phase shifter using substrate integrated waveguide," *IET Microw. Antennas Propag.*, vol. 6, no. 9, pp. 1090-1094, 2012, doi: 10.1049/iet-map.2011.0380.

[34] H. Peng, P. Jiang, T. Yang, and H. Jin, "Continuously tunable SIW phase shifter based on the buried varactors," *IEICE Electron. Express*, vol. 12, no. 7, pp. 1-7, 2015.

[35] E. Sbarra, L. Marcaccioli, R. V. Gatti and R. Sorrentino, "Ku-band analogue phase shifter in SIW technology," in *Proc. 39th Eur. Microw. Conf. (EUMC)*, pp. 264-267, 2009, doi: 10.23919/EUMC.2009.5296285.

[36] Y. Ji, L. Ge, J. Wang, Q. Chen, W. Wu and Y. Li, "Reconfigurable phased-array antenna using continuously tunable substrate integrated waveguide phase shifter," *IEEE Trans. Antennas Propag.*, vol. 67, no. 11, pp. 6894-6908, Nov. 2019, doi: 10.1109/TAP.2019.2927813.

[37] Z. Rahimian Omam et al., "Tunable substrate integrated waveguide phase shifter using high dielectric constant slab," *IEEE Microw. Wirel. Compon. Lett..*, vol. 30, no. 5, pp. 485-488, May 2020, doi: 10.1109/LMWC.2020.2980264.

[38] J. H. Dang, R. C. Gough, A. M. Morishita, A. T. Ohta and W. A. Shiroma, "Liquid-metal-based phase shifter with reconfigurable EBG filling factor," *IEEE MTT-S Int. Microw. Symp. Dig.*, Phoenix, AZ, USA, pp. 1–4. May 2015, doi: 10.1109/MWSYM.2015.7167062.

[39] D. M. Hensley, C. G. Christodoulou and N. Jackson, "A stretchable liquid metal coaxial phase shifter," *IEEE Open Journal of Antennas and Propagation*, vol. 2, pp. 370-374, 2021, doi: 10.1109/OJAP.2021.3063289.

[40] S. Alkaraki, A. L. Borja, J. R. Kelly, R. Mittra and Y. Gao, "Reconfigurable liquid metal-based SIW phase shifter," *IEEE Trans. Microw. Theory Tech..*, vol. 70, no. 1, pp. 323-333, Jan. 2022, doi: 10.1109/TMTT.2021.3124797.

[41] S. N. McClung, S. Saeedi, and H. H. Sigmarsson, "Band-reconfigurable filter with liquid metal actuation," *IEEE Trans. Microw. Theory Tech..*, vol. 66, no. 6, pp. 3073-3080, June 2018, doi: 10.1109/TMTT.2018.2823307.

[42] Y. -W. Wu, Z. -C. Hao, M. -C. Tao, X. Wang and J. -S. Hong, "A simple and accurate method for extracting super wideband electrical properties of the printed circuit board," *IEEE Access*, vol. 7, pp. 57321-57331, 2019, doi: 10.1109/ACCESS.2019.2911616.

[43] N. Tiercelin, P. Coquet, R. Sauleau, V. Senez, and H. Fujita, "Polydimethylsiloxane membranes for millimeter-wave planar ultra flexible antennas," *J. Micromech. Microeng.*, vol. 16, no. 11, pp. 2389-2395, 2006.

[44] A. Chakraborty and B. Gupta, "Paradigm phase shift: RF MEMS phase shifters: an overview," *IEEE Microwave Mag.*, vol. 18, no. 1, pp. 22-41, 2017, doi: 10.1109/MMM.2016.2616155.

[45] T. Cole and S. Tang, "Liquid metals as soft electromechanica actuators," *Adv. Mater.*, vol. 3, no. 1, pp. 173-185, Nov. 2022, doi: 10.1039/D1MA00885D.